nature climate change

SUPPLEMENTARY INFORMATION

https://doi.org/10.1038/s41558-017-0008-6

In the format provided by the authors and unedited.

# Increasing frequency of extremely severe cyclonic storms over the Arabian Sea

**Hiroyuki Murakami[1,2]*, Gabriel A. Vecchi[3,4] and Seth Underwood[1]**

[1]National Oceanic and Atmospheric Administration/Geophysical Fluid Dynamics Laboratory, Princeton, NJ, USA. [2]Atmospheric and Oceanic Sciences Program, Princeton University, Princeton, NJ, USA. [3]Department of Geosciences, Princeton University, Princeton, NJ, USA. [4]Princeton Environmental Institute, Princeton University, Princeton, NJ, USA. *e-mail: hir.murakami@gmail.com

# Supplementary Information

# Increasing Frequency of Extremely Severe Cyclonic Storms over the Arabian Sea

Hiroyuki Murakami[1, 2], Gabriel A. Vecchi[3,4], and Seth Underwood[1]

[1] National Oceanic and Atmospheric Administration/Geophysical Fluid Dynamics Laboratory, Princeton, NJ, USA

[2]Atmospheric and Oceanic Sciences Program, Princeton University, Princeton, NJ, USA

[3]Department of Geosciences, Princeton University, Princeton, NJ, USA

[4]Princeton Environmental Institute, Princeton University, Princeton, NJ, USA

## Supplementary Table

**TABLE S1.** Mean DIMI and change for each season: (a) mean DIMI projected by 1860Cntl; (b) As in (a), but for 2015Cntl; (c) difference between 2015Cntl and 1860Cntl; and (d) level of statistical significance shown.

| | April–June | October–December |
|---|---|---|
| (a) Mean DIMI (1860Cntl) | –3.51 | –4.65 |
| (b) Mean DIMI (2015Cntl) | –3.33 | –4.12 |
| (c) Diff (2015Cntl–1860Cntl) | +0.18 | +0.53 |
| (d) Level of statistical significance | 93% | >99% |

# Supplementary Figures

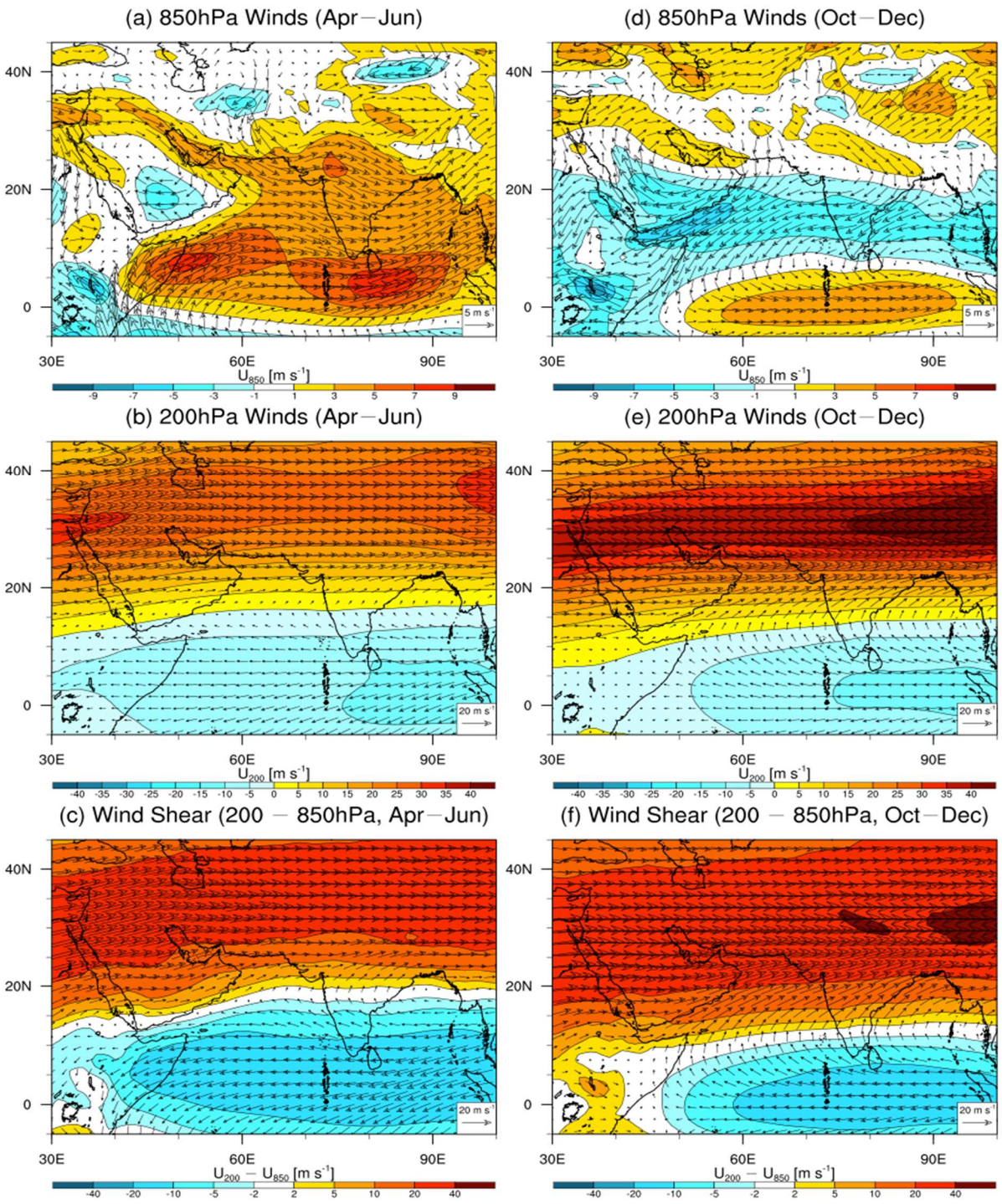


**Fig. S1** (a) Observed mean wind (vectors) and magnitude of zonal wind component at 850 hPa (shading) during the pre-monsoon season (April–June). (b) As in (a), but for 200 hPa. (c) Difference between (b) and (a), representing $V_s$. (d–f) As in (a–c), but for the post-monsoon season (October–December). Units: m $s^{-1}$. JRA-55[29] was used for the period 1980–2016.

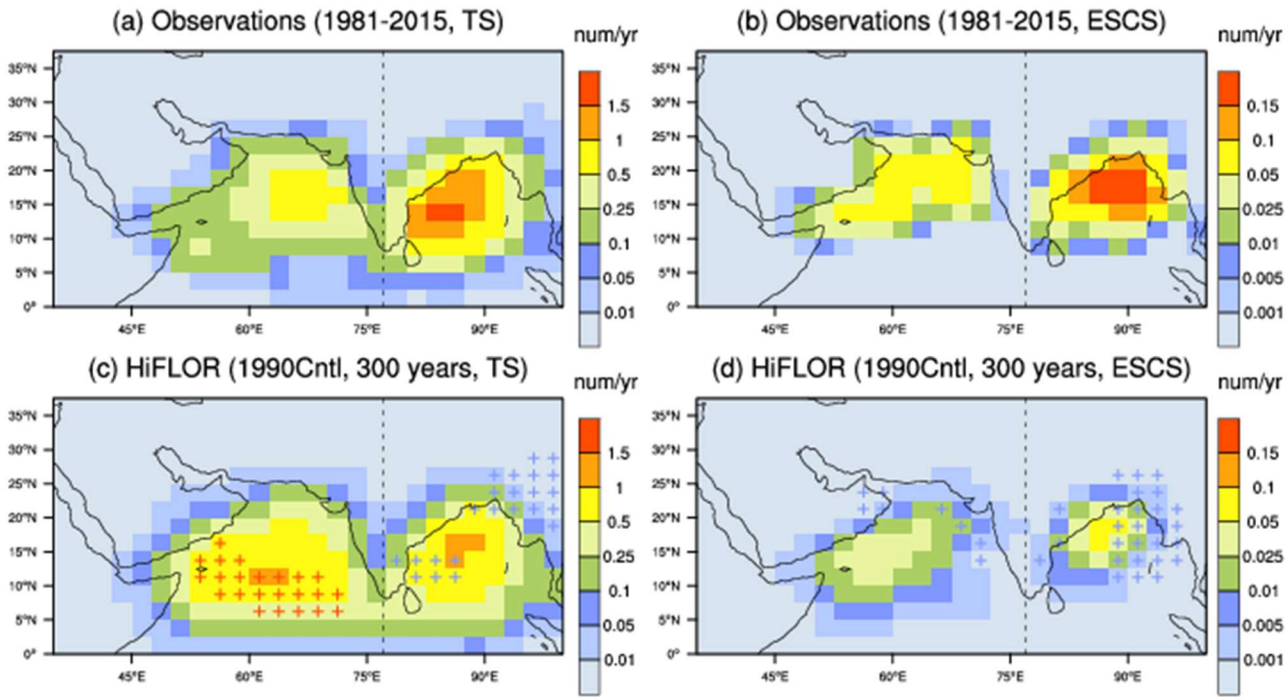


**Fig. S2** Annual mean density of tropical storms (≥17.5 m $s^{-1}$, left) and ESCSs (≥46.3 m $s^{-1}$, right) according to (a, b) observations (1981–2015)[25] and (c, d) 1990Cntl (300 years). The density is defined as the total count of storm position at 6-hr intervals in each 2.5° × 2.5°degree grid cell with 9-point weighting smoothing. Red (blue) cross marks in (c, d) indicate that the overestimation (underestimation) relative to the observed mean is statistically significant at the 99% confidence level or above (boot strap method proposed by Murakami et al.[24]). Panel (c) shows overestimation of tropical storms over the ARB and underestimation over the Bay of Bengal. Panel (d) indicates a reasonable distribution of ESCSs over the ARB, but an underestimation of ESCSs over the Bay of Bengal.

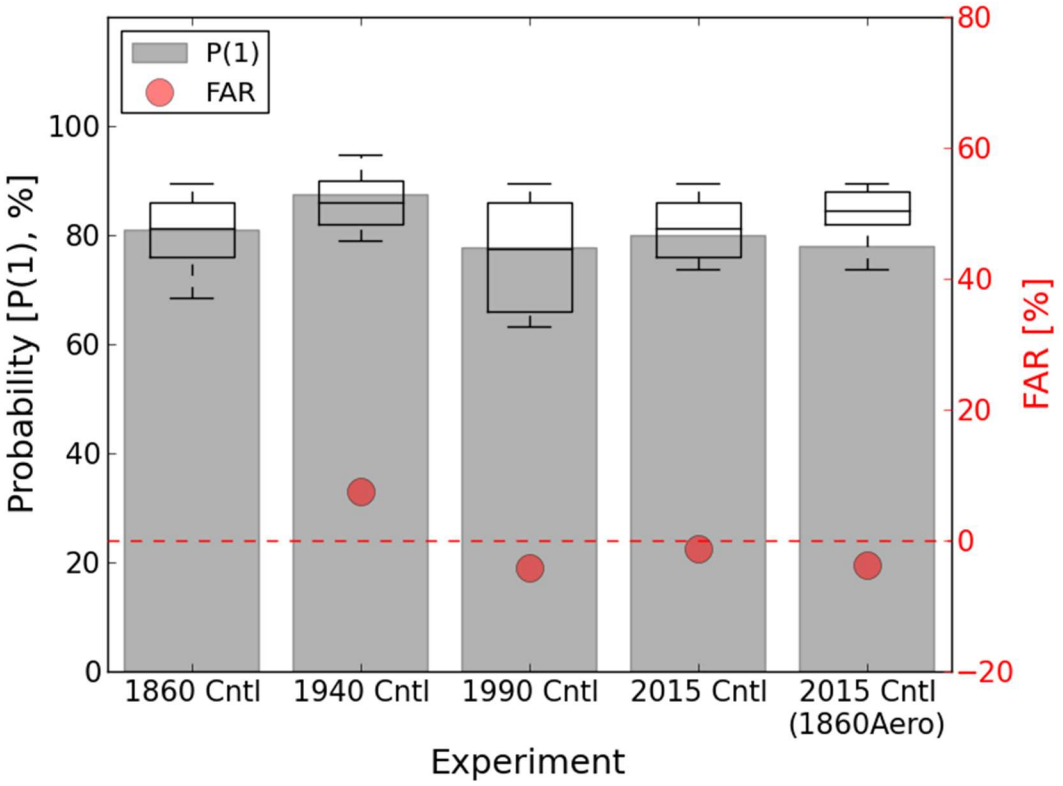


**Fig. S3** As in Fig. 3a in the main text, but for weak storms (< 46 m $s^{-1}$).

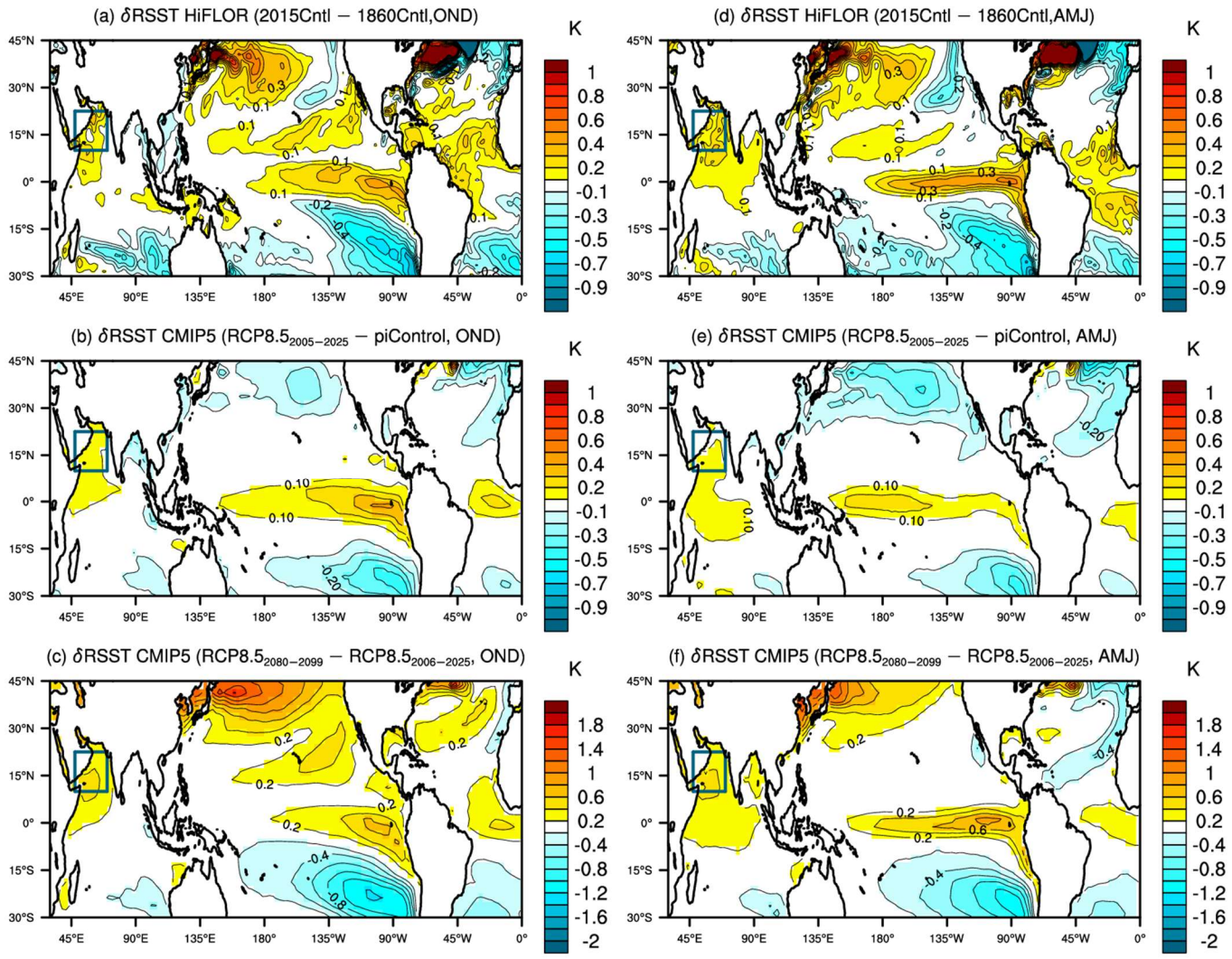


**Fig. S4** (a) Projected change in seasonal mean SST [K] relative to the tropical mean (30°S–30°N) change by 2015Cntl, relative to 1860Cntl, for October–December. (b) As in (a), but for the ensemble mean of 22 CMIP5 models under the RCP8.5 scenario (2006–2025) relative to those of the pre-industrial control experiments (500 years). (c) As in (a), but for the mean difference between 2080–2099 and 2006–2025 projected by 36 CMIP5 models under the RCP8.5 scenario. (d–f) As in (a–c), but for April–June. The green rectangle is the domain over the ARB where ESCSs increased.

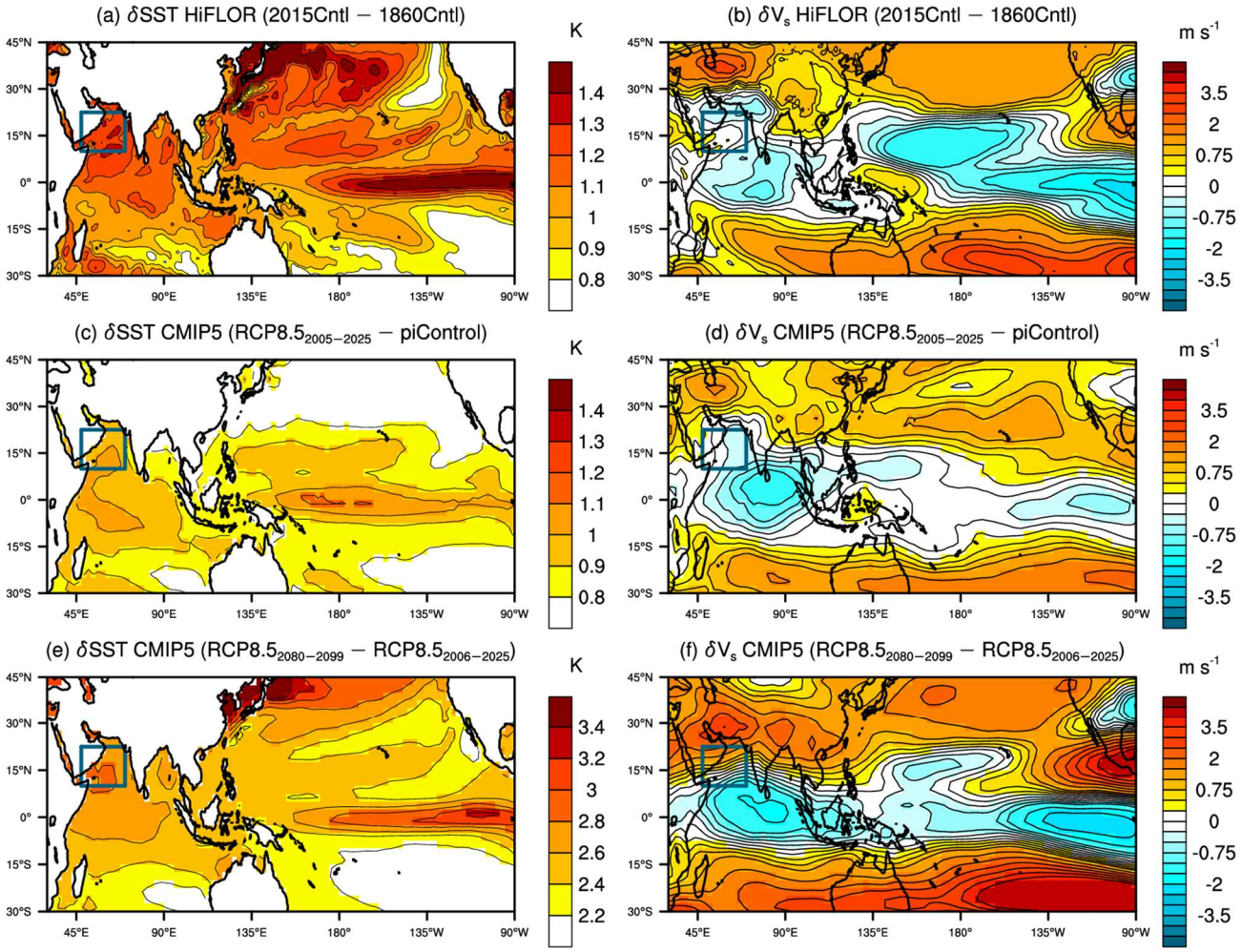


**Fig. S5** As in Fig. 4 in the main text, but for April–June.

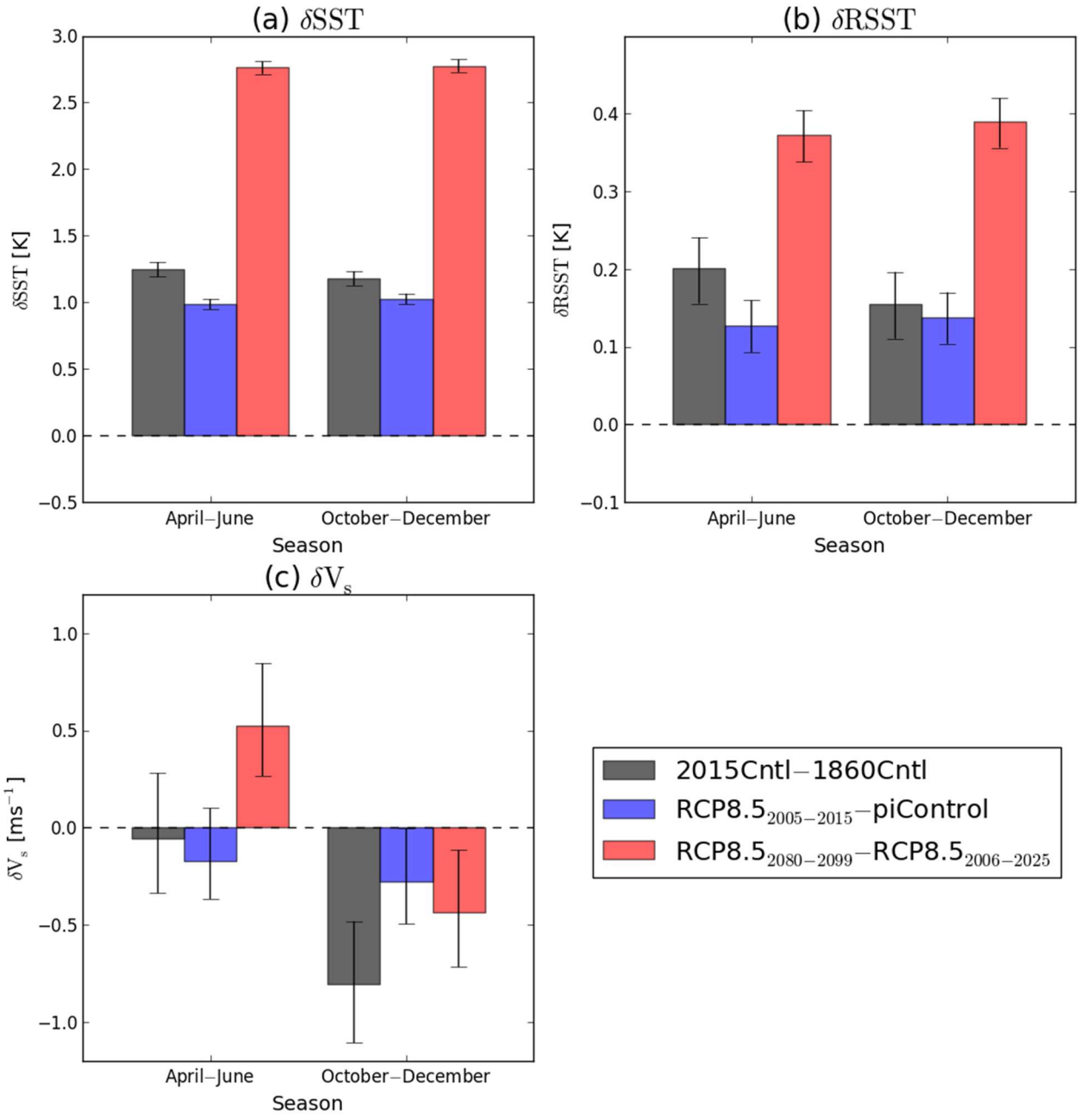


**Fig. S6** Area-mean of projected change in (a) SST, (b) RSST, and (c) $V_s$ over the domain where ESCSs increased (black rectangle in Fig. 2) for each season of April–June and October–December. Black bars show the changes in 2015Cntl relative to 1860Cntl. Blue bars show the changes in CMIP5 models under the RCP8.5 scenario (2006–2025) relative to those of the pre-industrial control experiments. Red bars show the difference between 2080–2099 and 2006–2025 projected by CMIP5 models under the RCP8.5 scenario. Error bars denote the 99% confidence interval computed by a bootstrap method[24].

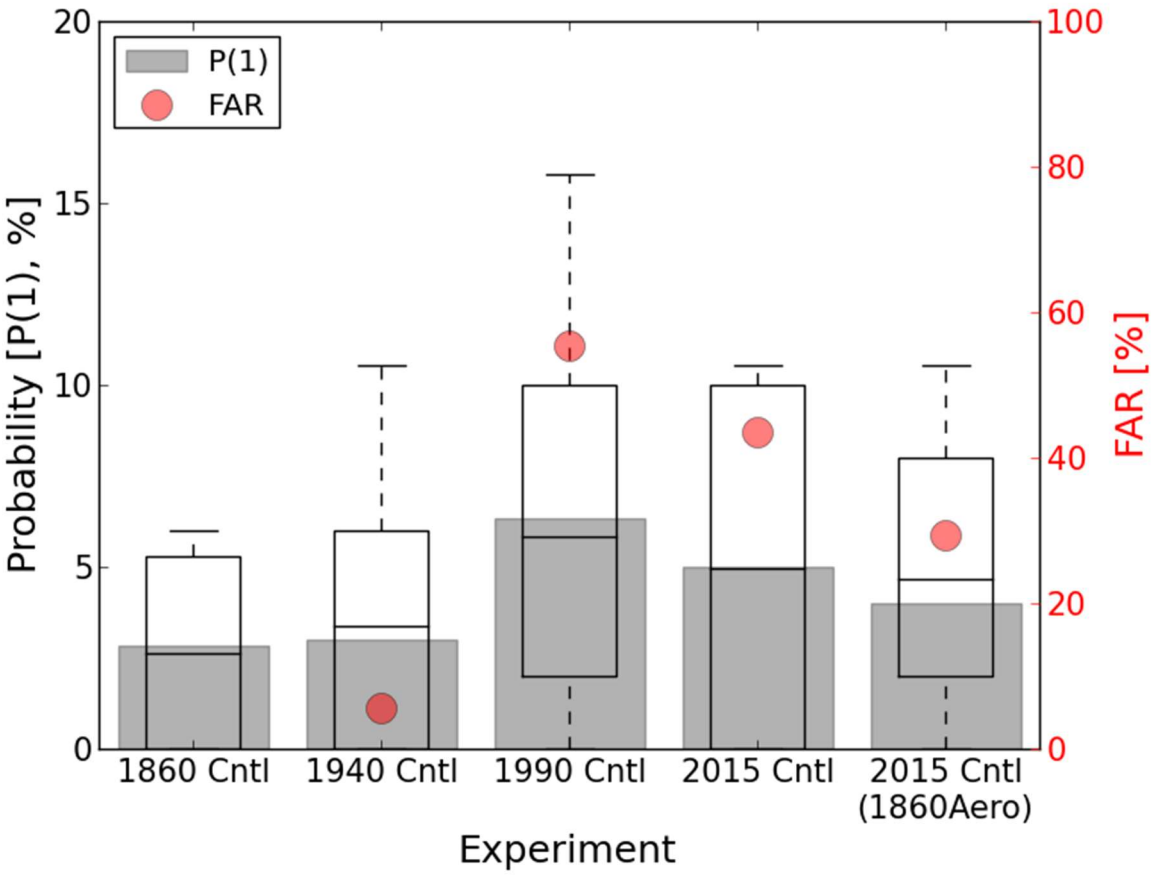


**Fig. S7** As in Fig. 3a in the main text, but for pre-monsoon season (April–June).

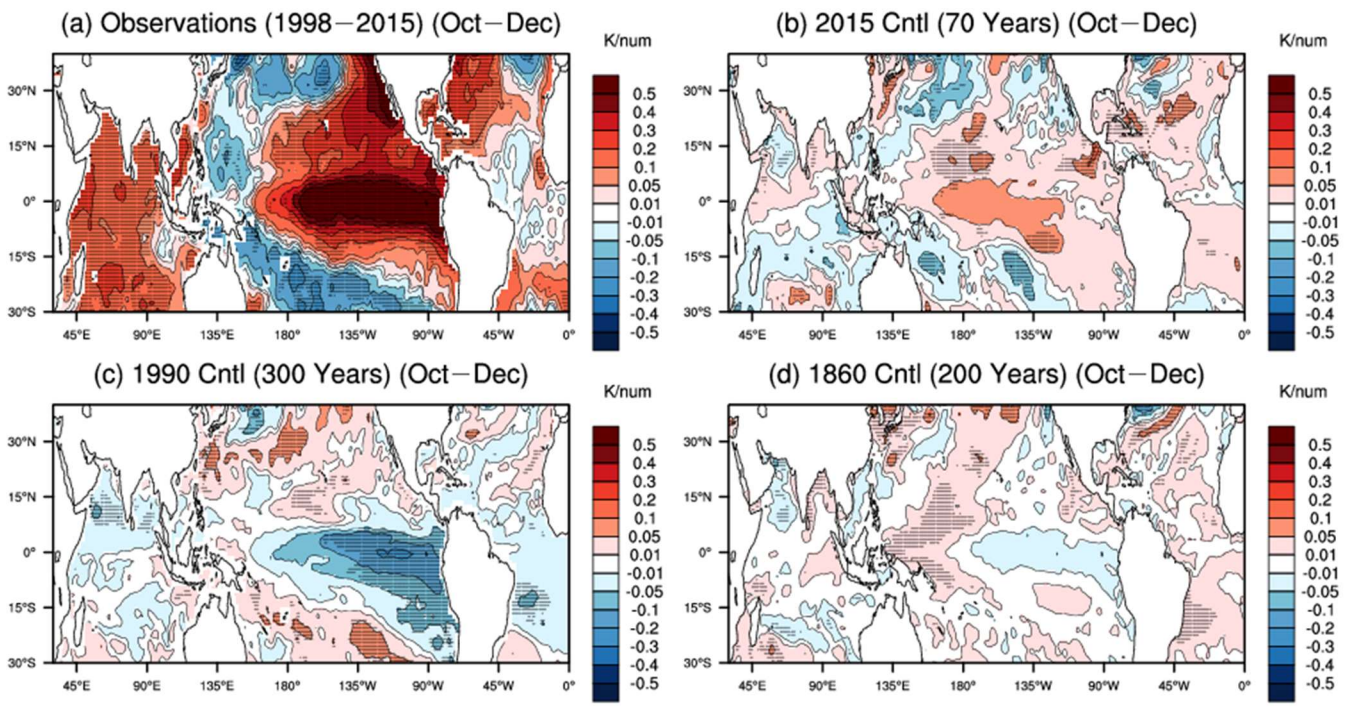


**Fig. S8** Regression of seasonal mean SST onto the number of ESCSs during the post-monsoon season (October–December). Units: K number$^{-1}$: (a) observations (1998–2015); (b) 2015Cntl (200 years); (c) 1990Cntl (300 years); (d) 1860Cntl (600 years). Cross marks indicate the value is statistically significant at the 90% confidence level. The observed regression map (a) suggests that ESCSs are more frequent when SSTs are warmer in the tropical and subtropical eastern Pacific as well as the Indian Ocean. This regressed spatial pattern reminds us of El Niño, a positive PDO, or a positive phase of the PMM. The regression map by 2015Cntl (b) indicates a similar pattern to the observations, although a maximum SST anomaly is located in the tropical central Pacific in addition to negative SST anomalies over the South Indian Ocean. On the other hand, 1990Cntl (c) and 1860Cntl (d) show spatial patterns opposite to the observations and 2015Cntl. They indicate that ESCSs are more frequent during La Niña.

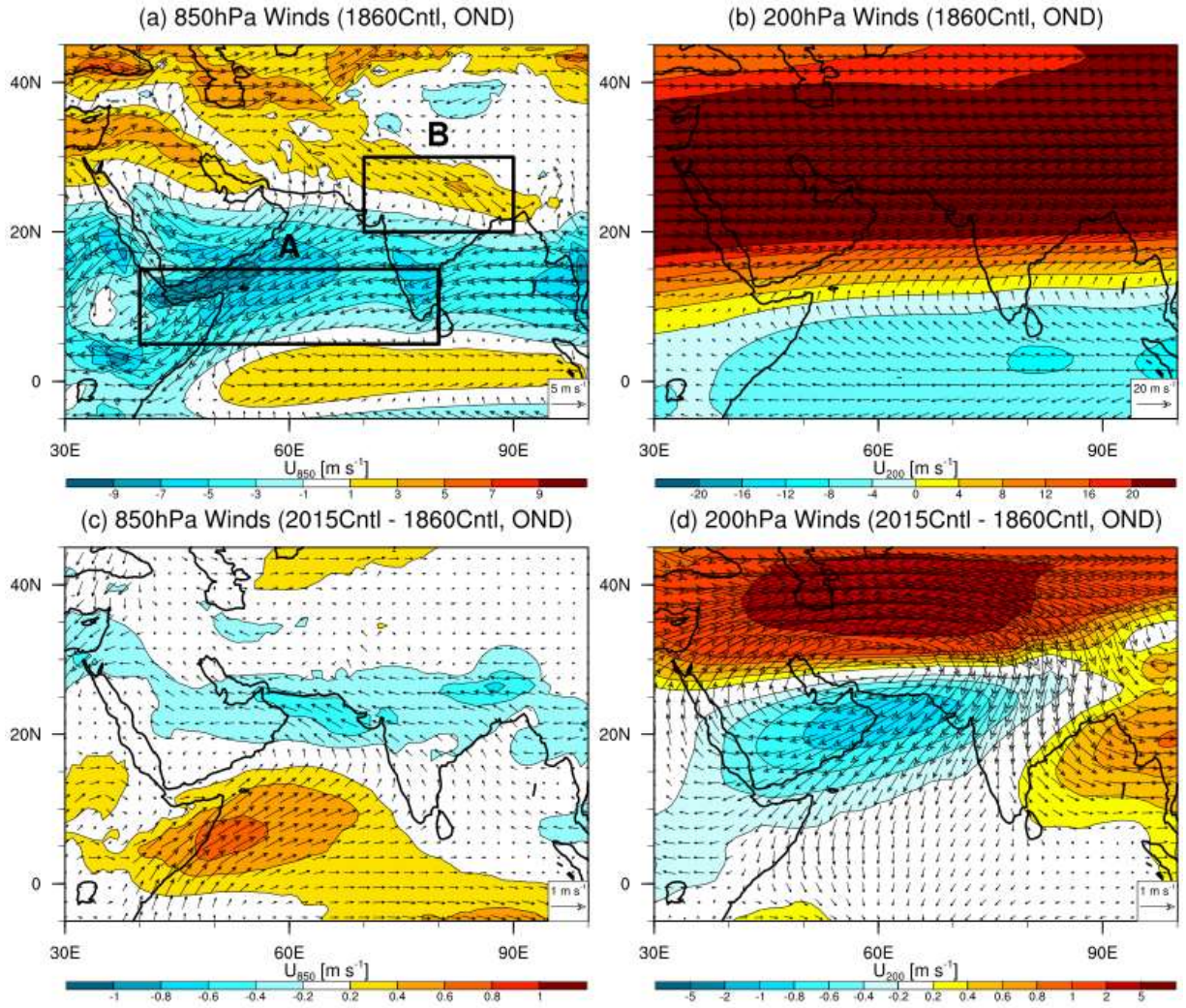


**Fig. S9** (a) Simulated mean winds (vectors) and zonal component of winds (shading) at 850 hPa by 1860Cntl during the post-monsoon season (October–December). (b) As in (a), but for 200 hPa. (c, d) As in (a, b), but for the projected changes by 2015Cntl relative to 1860Cntl. Rectangle domains in (a) are used to compute DIMI (see Methods). Units: m $s^{-1}$.

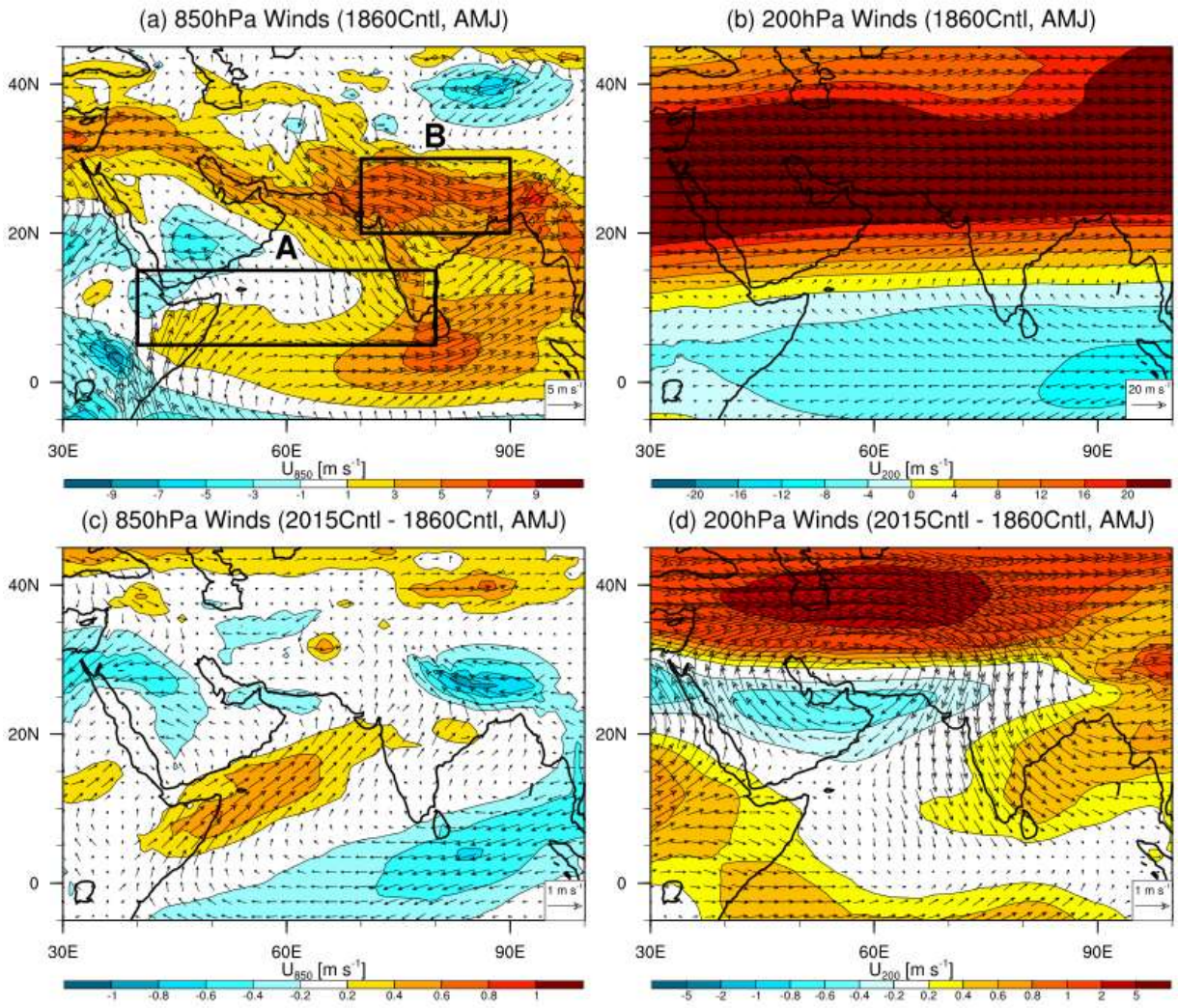


**Fig. S10** As in Fig. S8, but for pre-monsoon season (April–June).

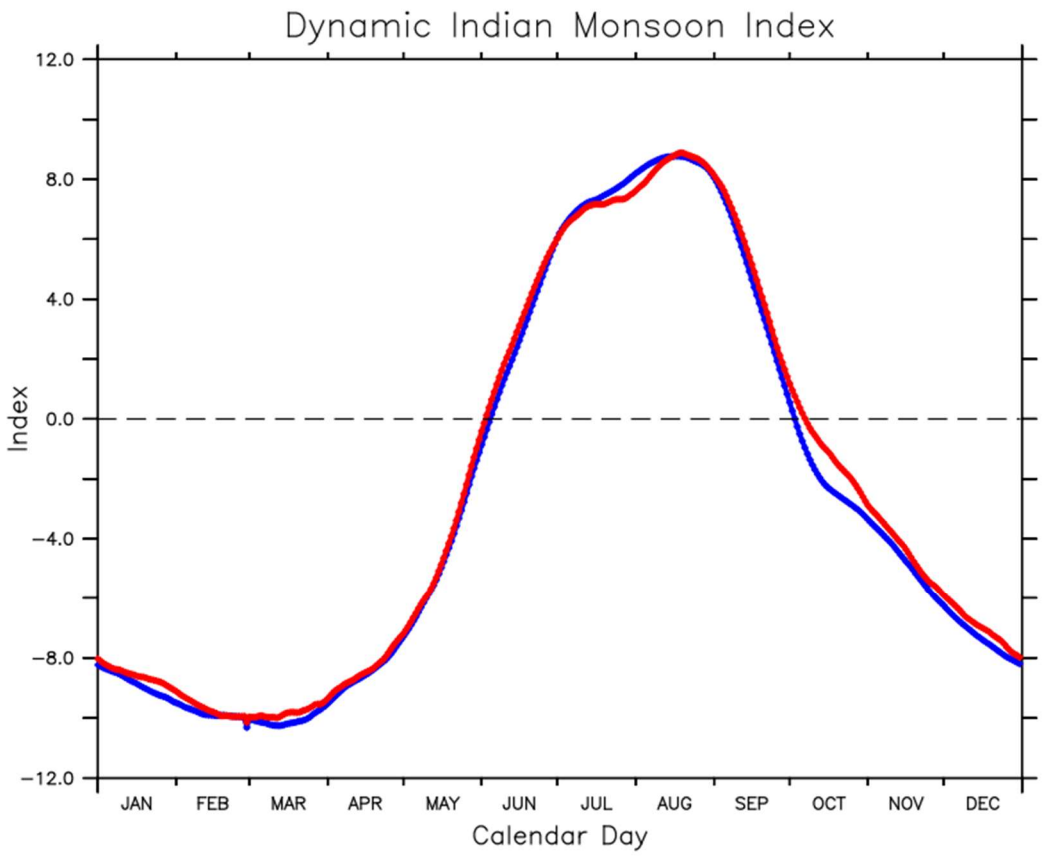


**Fig. S11** Simulated climatological daily mean of the 15-day running mean DIMI. Blue line is according to 1860Cntl; red line is according to 2015Cntl.

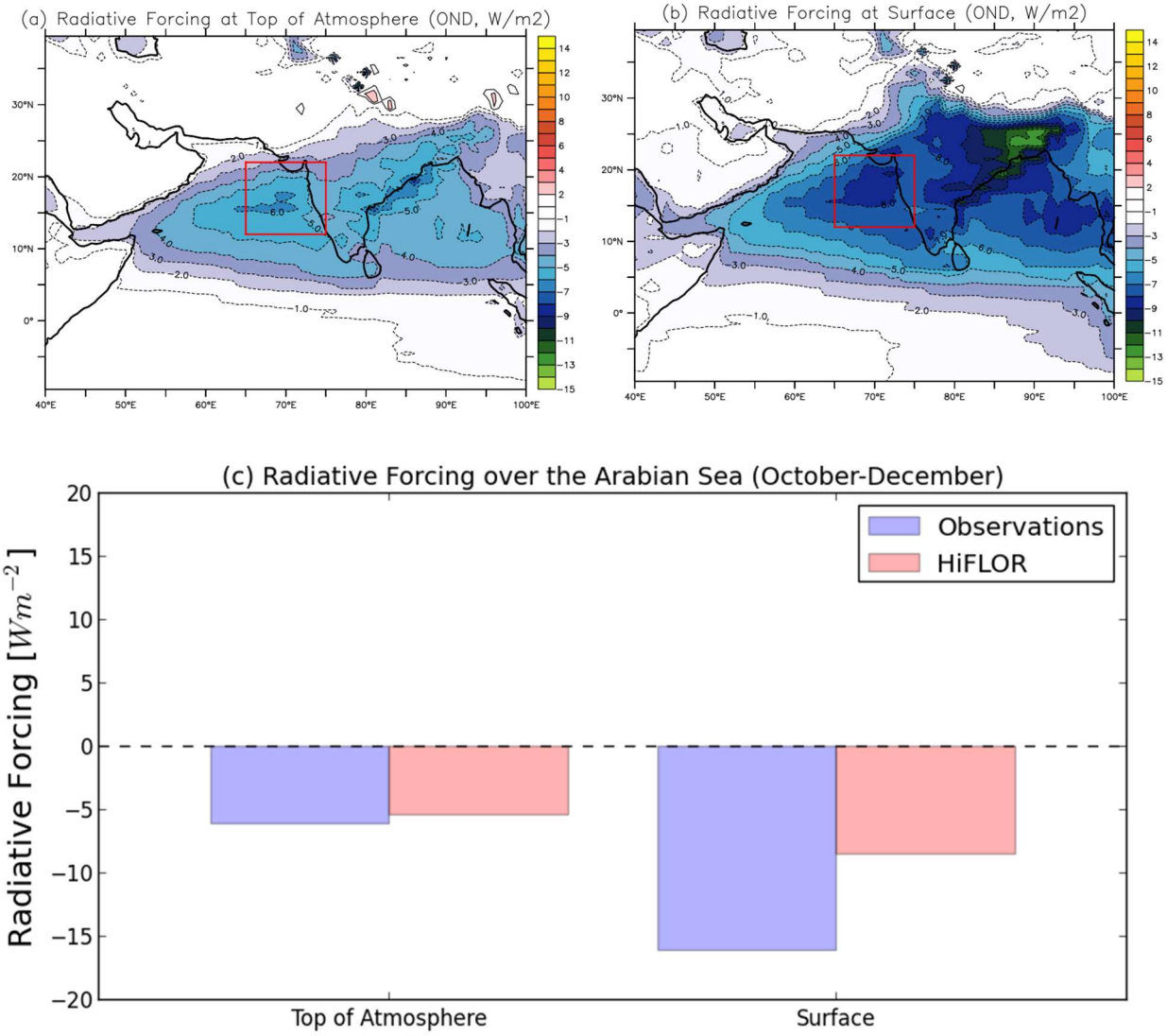


**Fig. S12** Radiative forcing of the aerosol–radiation interaction computed by the HiFLOR idealized experiment during the post-monsoon season (October–December) at the (a) top of the atmosphere and (b) surface. (c) Domain-mean radiative forcing over the ARB, denoted by the red rectangles in (a, b), computed by HiFLOR (red) and observations (blue) reported by Satheesh et al.[35]. Units: W $m^{-2}$.

## Supplemental Reference

35. Satheesh, S.K., K. K. Moorthy, Y.J. Kaufman & T. Takemura. Aerosol optical depth, physical properties and radiative forcing over the Arabian Sea. *Meteor. Atmos. Phys.*, **91,** 45–62 (2006).